Deblending in various domains

Ziguang Su and Daniel Trad

ABSTRACT

Seismic acquisition is a trade-off between economy and quality. Deblending of simultaneous source data, which allows a temporal overlap between shot records, has significant advantages to improve data quality (e.g., denser shooting) and reduce acquisition cost (e.g., efficient wide-azimuth shooting). Deblending may use the coherency property of simultaneous source data that varies in different domains. Common shot gathers (CSGs) can be converted into common midpoint gather, common receiver gather, or common image gather for deblending. Angle domain common image gathers (ADCIGs) can be extracted from Poynting vector or energy norm in reverse time migration(RTM). This report investigates blended data in the common image domain and creates an angle-related deblending method in ADCIGs.

INTRODUCTION

The blended acquisition technique targets at removing the limitation of no interference between adjacent shots by allowing sources to be shot simultaneously (Berkhout et al., 2009). The largest issue in simultaneous-source processing is intense crosstalk noise between adjacent shots, which poses a challenge for conventional processing (Chen et al., 2014).

Common image gathers are an important output of prestack depth migration. They not only can provide a velocity model for depth migration, but also can provide amplitude and phase information for subsequent subsurface attribute interpretation. Offset domain common image gathers (ODCIGs) and ADCIGs are seismic images organized by offset or incidence angle respectively at the reflection point.

Offset domain common image gather

ODCIGs are useful for migration velocity analysis and amplitude variation-to-offset (AVO) studies.

The offset in ODCIG normally refers to the distance between the shot and receiver on the surface. Later the concept of offset was extended to the subsurface offset between the upgoing and downgoing wavefields (Rickett and Sava, 2002), as shown in Fig 1. Offset changes from a data-space parameter to a model-space parameter by migration. In a reflection raytrace, the subsurface offset is continuous as the depth increases. The ODCIGs can be produced by either Kirchhoff migration or wavefield continuation migration (Sava and Fomel, 2003).

Angle domain common image gather

Angle domain common image gathers are a seismic slices recorded along reflection angle for each image point. Similar to ODCIGs, the ADCIGs can also be produced by

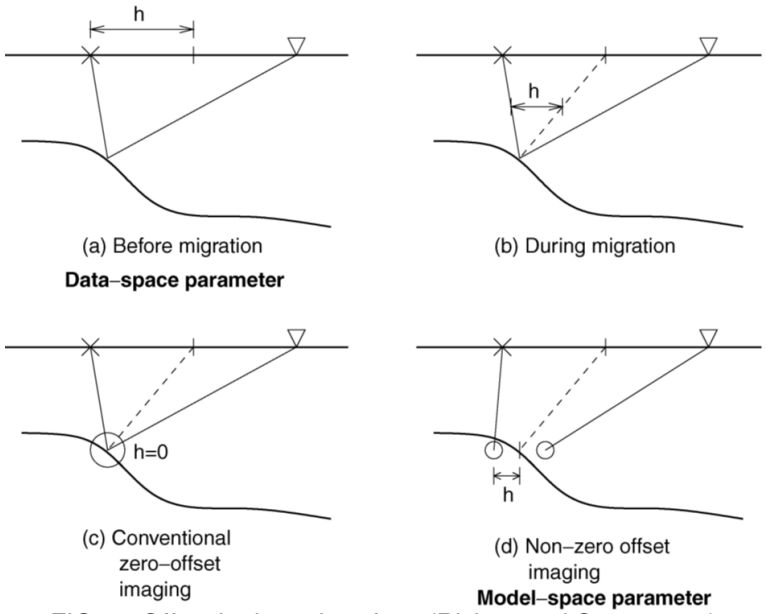

FIG. 1. Offset in the subsurface (Rickett and Sava, 2002)

pre-imaging methods like Kirchhoff methods (Xu et al., 2001) or wave-equation methods (De Bruin et al., 1990). These two methods are based on the wave equation, so there's no sensitivity to the ray-traced angle. The ADCIG can also be computed after-imaging (Biondi and Shan, 2002; Rickett and Sava, 2002) or transferred from ODCIG by Fourier Transform (Sava and Fomel, 2003).

Blended acquisition

A suitable method to reduce acquisition costs is to employ blended acquisition. While conventional acquisitions record energy coming from only one source at a time, blended acquisitions record energy coming from multiple sources simultaneously (Garottu, 1983; Beasley et al., 1998; Berkhout, 2008), as shown in Figure 2. We call the shot record of blended acquisition "supershot". Compared with the traditional acquisition method, blending acquisitions can save time and achieve denser shot density. On the other hand, seismic processing normally requires unblended shot records, so deblending with different methods (Berkhout, 2008; Mahdad et al., 2011; Akerberg et al., 2008; Beasley, 2008; Abma and Yan, 2009) was introduced to separate supershots into single shots. To facilitate deblending, often shots are fired with some random time delay between them (Berkhout et al., 2009; Mahdad et al., 2011). Simultaneous source data (also called blended data) can be synthesized from the non-overlapping (conventional) sources data by the following equation

$$b = \Gamma D \tag{1}$$

where b is the blended data, D represents the non-overlapping sources data cube, and Γ is the blending operator representing the sources firing times (Berkhout, 2008). Blended data b can be separated using the adjoint operator of the blending operator (called pseudo-deblending operator)

$$D' = \Gamma^T b \tag{2}$$

where D' is the pseudo-deblended data cube.

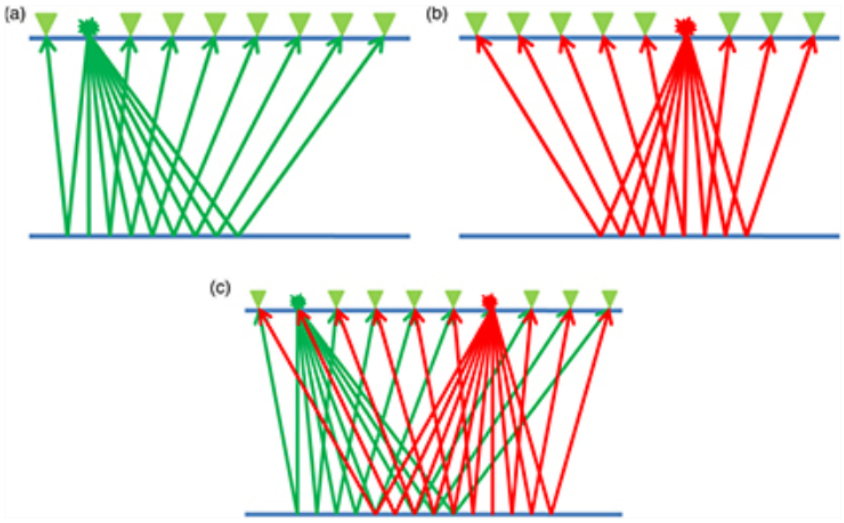

FIG. 2. (a) and (b) are illustrations of conventional single shot acquisition and (c) is blended shot acquisition.

For shots with time delays, it is possible to separate blended shots by converting from the shot domain to other domains. Unless the time delays are removed, seismic events are incoherent across traces that contain different shots (and therefore different time delays). For example, this happens in the midpoint, receiver, common offset, azimuth vectors, angle domain, and offset domains.

For each target shot in one supershot, there is a set of dithering time delays. Consequently, the size of the data increases by n_{blend} times, where n_{blend} is the number of sources simultaneously. Utilizing time delays, we could remove the corresponding time delay for each shot inside each "supershots." The target shot that sets the delay time is the shot we want to separate, and all the other shots are unwanted noise. In that way, we dither each shot record in the shot domain and add zero paddings for the blank. After dithering, the target shot turns coherent while all the other shots remain incoherent in other domains because delay time only fits with the target shot.

METHOD

Deblending using RTM

RTM is a migration method that is based on the two-way wave equation. Compared with migration methods based on the one-way wave equation, RTM has better results for complex structures like salt structures. RTM is initially introduced by many authors (Baysal et al., 1983; Whitmore, 2005; McMECHAN, 1983).

The concept of deblending by migration/demigration is that Green functions can act as basis functions onto which we can decompose the seismic data, independently of whether data are blended or not. In previous work, this has been done with Stolt operators (Trad et al., 2012; Ibrahim and Sacchi, 2015), but in those cases, the basis functions were more akin to apex shifted hyperbolas that represent true scatter responses. In deblending by migration,

we map the blended data to their true location since RTM can naturally handle simultaneous shots. The cross-correlation imaging condition automatically deblends blended energy. Although some crosstalk remains, that can be taken care of using least-squares reverse time migration (LSRTM). Therefore, the blended energy is mapped to the correct reflector model, which can be used to predict the data to any arbitrary acquisition geometry, as it has also been done for data regularization (Trad, 2015). Demigrating the estimated RTM image to individual shots rather than supershots produces unblended data. The quality of deblending and migration is related to the incoherency of blending interferences in the common receiver domain. The incoherency of the blending interferences is related to the randomness (dithering) of the shots.

The ADCIG can be obtained in RTM using flux density vector(Poynting vector).

Angle domain common image gather from Poynting vector

One method for extracting ADCIG during RTM is utilizing the Poynting vector (Dickens and Winbow, 2011).

The Poynting vector represents the directional energy flux of a wavefield (Stratton, 2007). The Poynting vector computation in seismic wavefield is

$$\mathbf{S} = -\upsilon P = -\nabla P \frac{dP}{dt} P \tag{3}$$

where $\mathbf{S}$ is the Poynting vector, $-\upsilon$ is the velocity vector and P is the stress wavefield (Cerveny, 2005). The $\mathbf{S}$ shares the same direction with the ray trace, so the angle between $\mathbf{S}_{source}$ and $\mathbf{S}_{receivers}$ is twice the value of reflection value.

$$cos2\theta = \frac{\mathbf{S}_{source}\mathbf{S}_{receivers}}{|\mathbf{S}_{source}||\mathbf{S}_{receivers}|} \tag{4}$$

where θ is the reflection angle. so the θ is

$$\theta = \frac{1}{2} arccos \frac{\mathbf{S}_{source}\mathbf{S}_{receivers}}{|\mathbf{S}_{source}||\mathbf{S}_{receivers}|} \tag{5}$$

In 2D, if we set the source stress wavefield as P_s and receiver stress wavefield as P_r, the refelction angle θ turns into

$$\theta = \frac{1}{2} arccos \frac{\frac{dP_s}{dx}\frac{dP_r}{dx} + \frac{dP_s}{dz}\frac{dP_r}{dz}}{\sqrt{(\frac{dP_s}{dx})^2 + (\frac{dP_s}{dz})^2} + \sqrt{(\frac{dP_r}{dx})^2 + (\frac{dP_r}{dz})^2}} \tag{6}$$

and vector perpendicular to the reflection plane is

$$\mathbf{S} = (\mathbf{S}_{source} + \mathbf{S}_{receivers})/|cos2\theta| \tag{7}$$

The azimuth can also be computed, and in the 2D case, it is either 0° or 180°. With the angle information, the common angle gather can be obtained after RTM without external computation. The result of normal RTM is the cross-correlation of shot wavefield and receiver wavefield. It is the summation of all angle gathers. To get the ADCIG, the reflection angle θ is introduced in RTM's image condition.

Angle domain common image gather from energy norm

In this section, the energy-norm imaging condition is derived using an analytical wavefield (Sun et al., 2017). The energy norm with respect to a symmetric positive definite (SPD) matrix M can be defined as:

$$e^2(\mathbf{u}) = ||\mathbf{u}||_{\mathbf{M}} = \mathbf{u}^\intercal \mathbf{M}\mathbf{u} \ . \tag{8}$$

where $\mathbf{u}$ is the wavefield.

In the acoustic case, the imaging condition based on the energy-norm is also referred to as the impedance sensitivity kernal (Zhu et al., 2009) or the inverse scattering imaging condition (Whitmore and Crawley, 2012):

$$I_a = \rho \mathbf{u}_t^\intercal \mathbf{w}_t + (v\nabla \mathbf{u})^\intercal (v\nabla \mathbf{w}) \ . \tag{9}$$

where ρ is density, t is time,$\mathbf{u}$ and $\mathbf{w}$ is the forward and backward wavefield. $\mathbf{u}_t = \partial \mathbf{u}/\partial t$.

For general elastic media, the energy norm imaging condition can be expressed as (Kiyashchenko et al., 2007; Rocha et al., 2016)

$$I_e = \rho \mathbf{u}_t^\intercal \mathbf{u}_t + \mathbf{u}^\intercal \mathbf{D}\mathbf{C}\mathbf{D}^\intercal \mathbf{u} \ . \tag{10}$$

It is important to note that the inverse and forward scattering imaging conditions using scalar and vector analytical wavefields discussed in this section are not restricted to one-step wave extrapolation. There are different ways of obtaining an analytical wavefield using conventional finite-different or pseudo-spectral wave extrapolation, for example, by separately propagating a wavefield using a Hilbert-transformed source wavelet (Shen and Albertin, 2015; Hu et al., 2016) and using it as the imaginary part of the analytical wavefield.

Deblending from common image gather

The common image gather can be utilized in the deblending algorithm. In blended acquisition, forward energy coming from different sources has various reflection angles at the image point. The ADCIG calculated from the Poynting vector or energy norm could deblend the blended gathers by separating waves with different reflection angles.

The reflection angle is computed from the wave direction vector in the source and receiver wavefield. This paper improves the angle calculating algorithm from the conventional computation 5 to the clockwise angle computation, as shown in Figure3. The shot energy coming from different sides of the image point has opposite rotation direction angles. One is clockwise and the other is counterclockwise. The cross-product of the two vectors could compute the clockwise/ counterclockwise property, as shown in equation 11.

$$sin2\theta = \frac{\mathbf{S}_{source} \times \mathbf{S}_{receivers}}{|\mathbf{S}_{source}||\mathbf{S}_{receivers}|} \tag{11}$$

$$\theta = \frac{1}{2} arcsin \frac{\mathbf{S}_{source} \times \mathbf{S}_{receivers}}{|\mathbf{S}_{source}||\mathbf{S}_{receivers}|} \tag{12}$$

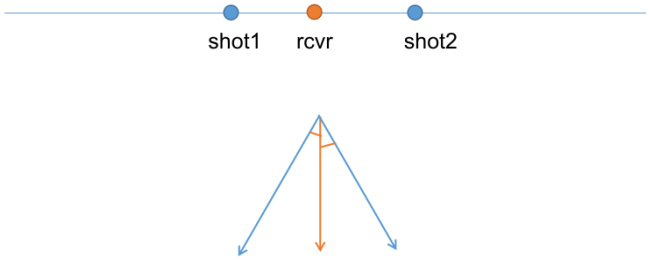

FIG. 3. Reflection angle is the angle between the incident vector and the reflected vector. One angel is clockwise while the other is counterclockwise.

In 2D, if we set the source stress wavefield as P_s and receiver stress wavefield as P_r, the reflection angle θ turns into

$$\theta = \frac{1}{2} arccos \frac{\frac{dP_s}{dx}\frac{dP_r}{dz} - \frac{dP_s}{dz}\frac{dP_r}{dx}}{\sqrt{(\frac{dP_s}{dx})^2 + (\frac{dP_s}{dz})^2}\sqrt{(\frac{dP_r}{dx})^2 + (\frac{dP_r}{dz})^2}} \tag{13}$$

and vector perpendicular to the reflection plane is

$$\mathbf{S} = (\mathbf{S}_{source} + \mathbf{S}_{receivers})/|sin2\theta| \tag{14}$$

The cross-product of the two vectors can be positive or negative, which indicates the clockwise/counter-clockwise reflection angle. The cross product could only compute the angle from 0 to 90 degrees while the dot product in equation 4 could cover the angle from 0 to 180 degrees.

RESULTS AND DISCUSSION

A five-layered velocity model is used to examine the results, as shown in Figure 4. There are 800 data points both vertically and horizontally. The grid size is 5x5 meters. The internal velocities in each layer are 1.5, 1.6, 1.7, 1.8, and 1.9 km/s respectively from surface to bottom. For all the acquisition coordinates, there are 800 geophones on the surface.

In the unblended acquisition coordinates, the shot interval is 40 meters. The ADCIGs computed from the Poynting vector are shown in Figure 5, the energy norm one has the same results. It can be seen that all 4 reflectors are displayed clearly, but the amplitude at all layers vary as the angle changes, except the most shadow reflector. Generally, small angles have higher amplitudes compared to the large angles. The high amplitude zone moves towards a small angle direction as the depth increases, which corresponds to the reality that the reflection angle decreases as depth increases. There is an outlier area at the top right corner, which shows the ADCIG is limited in shadow depth for large reflection angles. There are large artifacts on 80 degrees from 0.2km to 0.8km. The reason for that remains unclear. In the blended acquisition coordinates, the shot interval is also 40 meters, but two sources are shot simultaneously at a constant distance of 400 meters. The ADCIG for blended acquisition is shown in Figure 6. It can be seen that the blended ADCIG has a higher amplitude and large angle coverage than the unblended one, that's because the energy ejected into the subsurface is double the quantity of the unblended acquisition

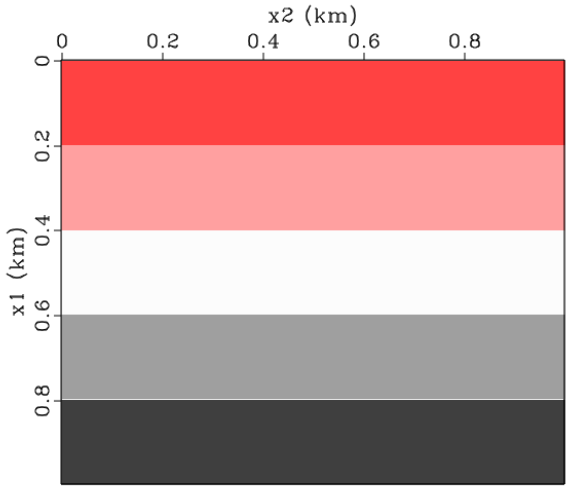

FIG. 4. 5-layered velocity model.

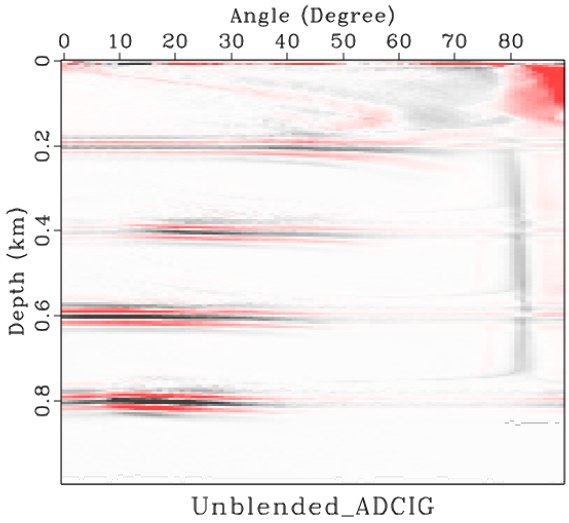

FIG. 5. ADCIG for unblended data.

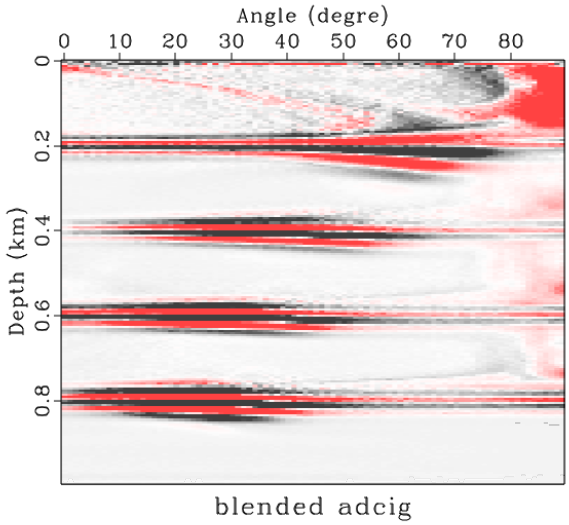

FIG. 6. ADCIG for blended data

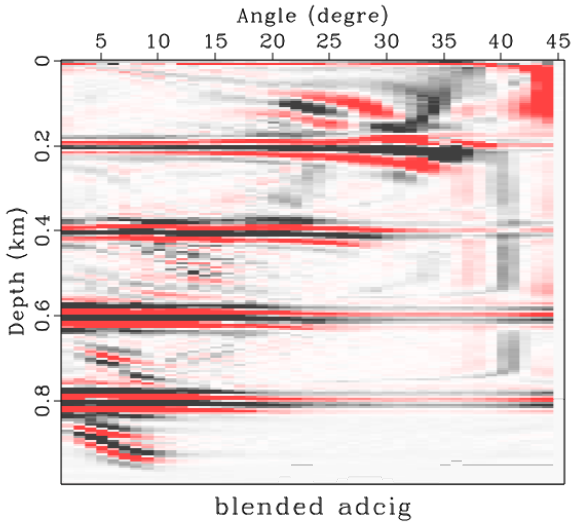

FIG. 7. ADCIG for deblended data1.

and larger offset, which enhance the data quality. The artifact in 80 degrees doesn't exist in the blend ADCIG, indicating the blended acquisition could attenuate some unwanted noise. The outlier area at the top right corner is not as apparent as the unblended one, we could distinguish the reflector below the outlier. Similar to the unblended ADCIG, all 4 reflectors are displayed clearly, and the amplitude at each layer varies as the angle changes. The high amplitude zone moves towards a small-angle direction as the depth increases. Using the deblending algorithm from equation 3, the blended ADCIG can be deblended into to deblended ADCIG, as shown in Figure 7 and 8. It can be seen that the deblended ADCIG is not as sharp as the blended ADCIG. The two deblended ADCIG are exactly alike because the acquisition coordinate is symmetric, but one is clockwise angle and the other is counterclockwise. There are unwanted noises between the reflectors. One possible source of the noise can be the crosstalk between the sources. And the artifacts attenuated by blending in the 80 degrees exist again.

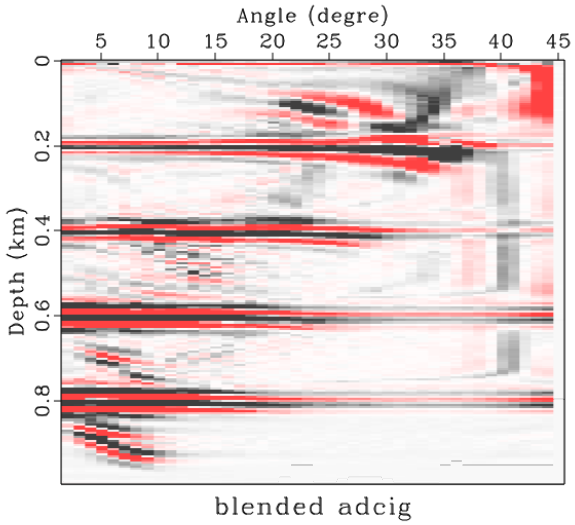

FIG. 8. ADCIG for deblended data2.

CONCLUSIONS

Simultaneous-source acquisition could improve data quality and reduce acquisition costs. Offset and angle domain common image gathers are an important output of prestack depth migration. The ADCIG can be derived from the Poynting vector or energy norm in RTM. Blended acquisition in ADCIG could attenuate noise, increase angle coverage, and improve image quality. The deblending algorithm in ADCIG is not perfect: it would recover the noise attenuated by blending and create noise by the crosstalk of different sources. But it can deblend energy coming from a different angle of the image point.

ACKNOWLEDGMENTS

We thank the sponsors of CREWES for their continued support. This work was funded by CREWES industrial sponsors and NSERC (Natural Science and Engineering Research Council of Canada) through the grant CRDPJ 543578-19.

REFERENCES

Abma, R., and Yan, J., 2009, Separating simultaneous sources by inversion, *in* 71st EAGE Conference and Exhibition incorporating SPE EUROPEC 2009.

Akerberg, P., Hampson, G., Rickett, J., Martin, H., and Cole, J., 2008, Simultaneous source separation by sparse radon transform, *in* SEG Technical Program Expanded Abstracts 2008, Society of Exploration Geophysicists, 2801–2805.

Baysal, E., Kosloff, D. D., and Sherwood, J. W. C., 1983, Reverse time migration: GEOPHYSICS, **48**, No. 11, 1514–1524.

Beasley, C. J., 2008, A new look at marine simultaneous sources: The Leading Edge, **27**, No. 7, 914–917.

Beasley, C. J., Chambers, R. E., and Jiang, Z., 1998, A new look at simultaneous sources, *in* SEG Technical Program Expanded Abstracts 1998, Society of Exploration Geophysicists, 133–135.

Beasley, C. J., Dragoset, B., and Salama, A., 2012, A 3d simultaneous source field test processed using al-

ternating projections: A new active separation method: Geophysical Prospecting, **60**, No. 4-Simultaneous Source Methods for Seismic Data, 591–601.

Berkhout, A., 2008, Changing the mindset in seismic data acquisition: The Leading Edge, **27**, No. 7, 924–938.

Berkhout, A. J., Blacquière, G., and Verschuur, D. J., 2009, The concept of double blending: Combining incoherent shooting with incoherent sensing: GEOPHYSICS, **74**, No. 4, A59–A62.

Biondi, B., and Shan, G., 2002, Prestack imaging of overturned reflections by reverse time migration, Society of Exploration Geophysicists: SEG Technical Program Expanded Abstracts 2002, 1284–1287.

Cerveny, V., 2005, Seismic ray theory: Cambridge university press.

Chen, Y., Fomel, S., and Hu, J., 2014, Iterative deblending of simultaneous-source seismic data using seislet-domain shaping regularization: Geophysics, **79**, No. 5, V179–V189.

De Bruin, C., Wapenaar, C., and Berkhout, A., 1990, Angle-dependent reflectivity by means of prestack migration: Geophysics, **55**, No. 9, 1223–1234.

Dickens, T. A., and Winbow, G. A., 2011, Rtm angle gathers using poynting vectors, *in* SEG Technical Program Expanded Abstracts 2011, Society of Exploration Geophysicists, 3109–3113.

Garottu, R., 1983, Simultaneous recording of several vibroseis® seismic lines, Society of Exploration Geophysicists: SEG Technical Program Expanded Abstracts 1983, 308–310.

Hu, J., Wang, H., and Wang, X., 2016, Angle gathers from reverse time migration using analytic wavefield propagation and decomposition in the time domain: Geophysics, **81**, S1–S9.

Ibrahim, A., and Sacchi, M. D., 2015, Fast simultaneous seismic source separation using Stolt migration and demigration operators: Geophysics, **80**, No. 6, WD27–WD36.

Kiyashchenko, D., Plessix, R.-E., Kashtan, B., and Troyan, V., 2007, A modified imaging principle for true-amplitude wave-equation migration: Geophysical Journal International, **168**, 1093–1104, `http://gji.oxfordjournals.org/content/168/3/1093.full.pdf+html`.
URL `http://gji.oxfordjournals.org/content/168/3/1093.abstract`

Mahdad, A., Doulgeris, P., and Blacquiere, G., 2011, Separation of blended data by iterative estimation and subtraction of blending interference noise: Geophysics, **76**, No. 3, Q9–Q17.

McMECHAN, G. A., 1983, Migration by extrapolation of time-dependent boundary values*: Geophysical Prospecting, **31**, No. 3, 413–420.

Rickett, J. E., and Sava, P. C., 2002, Offset and angle-domain common image-point gathers for shot-profile migration: Geophysics, **67**, No. 3, 883–889.

Rocha, D., Tanushev, N., and Sava, P., 2016, Isotropic elastic wavefield imaging using the energy norm: Geophysics, **81**, S207–S219, `http://dx.doi.org/10.1190/geo2015-0487.1`.
URL `http://dx.doi.org/10.1190/geo2015-0487.1`

Sava, P. C., and Fomel, S., 2003, Angle-domain common-image gathers by wavefield continuation methods: Geophysics, **68**, No. 3, 1065–1074.

Shen, P., and Albertin, U., 2015, Up-down separation using Hilbert transformed source for causal imaging condition, *in* 85th Annual International Meeting, SEG, Expanded Abstracts, 4175–4179.

Stratton, J. A., 2007, Electromagnetic theory, vol. 33: John Wiley & Sons.

Sun, J., Fomel, S., Sripanich, Y., and Fowler, P., 2017, Recursive integral time extrapolation of elastic waves using low-rank symbol approximation: Geophysical Journal International, **211**, No. 3, 1478–1493.

Trad, D., 2015, Least squares kirchhoff depth migration: implementation, challenges, and opportunities, *in* 2015 SEG Annual Meeting, Society of Exploration Geophysicists, 4238–4242.

Trad, D., 2018, Compressive sensing, sparse transforms and deblending.

Trad, D., Siliqi, R., Poole, G., Boelle, J.-L. et al., 2012, Fast and robust deblending using apex shifted radon transform, Society of Exploration Geophysicists.

Whitmore, N., and Crawley, S., 2012, Applications of rtm inverse scattering imaging conditions, *in* SEG technical program expanded abstracts 2012, Society of Exploration Geophysicists, 1–6.

Whitmore, N. D., 2005, Iterative depth migration by backward time propagation: SEG Technical Program Expanded Abstracts 1983, 382–385, https://library.seg.org/doi/pdf/10.1190/1.1893867. URL https://library.seg.org/doi/abs/10.1190/1.1893867

Xu, S., Chauris, H., Lambaré, G., and Noble, M., 2001, Common-angle migration: A strategy for imaging complex media: Geophysics, **66**, No. 6, 1877–1894.

Zhu, H., Luo, Y., Nissen-Meyer, T., Morency, C., and Tromp, J., 2009, Elastic imaging and time-lapse migration based on adjoint methods: Geophysics, **74**, No. 6, WCA167–WCA177.